Nanomaterials

DOI: 10.1002/ange.201210277

Semiconducting and Plasmonic Copper Phosphide Platelets**

*Goutam Manna, Riya Bose, and Narayan Pradhan**

Designing different nanomaterials with new and useful properties required for developing day-to-day technologies has remained in the forefront of research for decades. Among these, semiconducting, light-emitting, plasmonic, photovoltaic, and magnetic properties are in the frontline.[1–13] Furthermore, materials with rectification properties remain one of the most demanding materials in recent times.[1–4,14–17] Very recently, semiconducting nanomaterials with tunable plasmonic absorption properties have also been reported;[5–8,18–22] these may further expand the already widespread applications of these nanomaterials in diverse research fields, including both in biology and device-based technologies. Hence, materials with several of these new properties are in demand for their implementation in different developing modern technologies.

For designing nanomaterials, the colloidal synthetic method has remained unique and unbeatable to date. However, the classical mechanistic approach for fabricating these materials following this solution phase synthesis is more effective for tuning over a smaller range of dimensions, and produces mostly smaller-sized nanocrystals. Efforts to get larger-sized nanocrystals lead either to a wider size distribution or precipitation. Generally, this has been observed for 0D, 1D, or 2D crystal-growth processes.[23–30] Hence, designing of surface-ligand-capped nanomaterials with a wide range of size tunability that maintains their narrow size distribution throughout still remains challenging and requires more advanced synthetic methods.

Confining the growth to 2D, we explore here the fabrication of nano- to microscale-tunable platelet-shaped Cu^{I} phosphide as one of the upcoming materials associated with several new properties. This shows the band-edge absorption in the NIR spectral window, tunable surface plasmonic absorption in mid-IR window and also has the rectification properties required for possible exploration as photovoltaic material. Synthesis with such a wide tunable size range (ca. 1000 nm) has been performed by controlling the number of nucleations followed by rapid growth along two feasible directions. In the entire tunable regime, the size distribution remains narrow; the platelets maintain a hexagonal shape and retain single crystallinity. Moreover, unlike reported nanoplatelets made from various materials, these show several intriguing patterns of Moiré fringes in their overlapping regions on the TEM grid. Finally, these p-type semiconducting platelets are explored to study their, photocurrent, photoresponse and photovoltaic activity under white-light illumination.

For the synthesis of copper phosphide, phosphine gas generated ex situ[31] has been explored as the phosphide source. This also helps to carry out the reaction at relatively moderate temperatures (200–230 °C). Using CuCl as Cu precursor, a mixture of alkylamine and trioctylphosphine-oxide as solvent, and trioctylphosphine as the nucleation controlling agent, different size of copper phosphide nanoplatelets ranging from ca. 10 nm width to ca. 1000 nm width are synthesized. The synthetic method adopted was somewhat different than the conventional colloidal method. In the latter case, nucleations and growth processes are normally decoupled to achieve the narrow size distribution, and time-dependent samples are collected to obtain the size tunable nanocrystals. On the other hand, we disclose here different reactions to control the formation of different numbers of nucleations, and the nanoplatelets are collected at certain fixed times. The synthetic procedure is shown in Figure 1 a and the reaction parameter variations are shown in Table S1 in the Supporting Information. Figure 1 b–g shows the different sizes of platelets, all of which attain a hexagonal shape and are obtained by controlling the density of nucleations in solution. From the concentrated samples, where the platelets

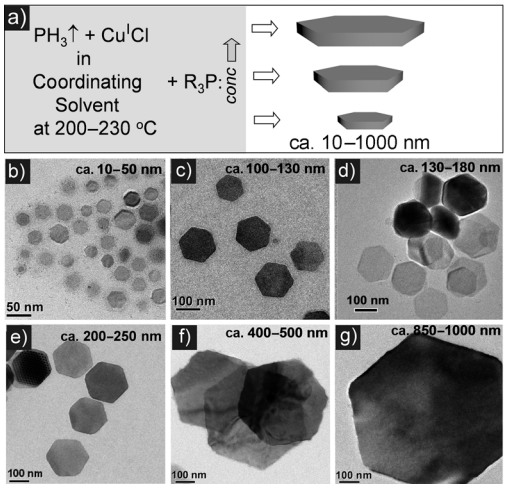

Figure 1. a) Reaction Scheme and the TOP (trioctylphosphine) concentration dependent tunability of the Cu_3P nanoplatelets width. b–g) TEM images of different Cu_3P platelet sizes obtained from different reactions. Details of the synthesis parameters for these platelets are provided in Table S1. The width can be controlled over the range of ca. 10–1000 nm over the range of reactions. For each case, the average width range has been labeled inside the panel. For more TEM images with low magnification, see Figure S1.

[*] G. Manna, R. Bose, Dr. N. Pradhan
Department of Materials Science and Centre for Advanced Materials, Indian Association for the Cultivation of Science
Kolkata-700032 (India)
E-mail: camnp@iacs.res.in

[**] This work was supported by DST and CSIR, India. Swarnajayanti Project and CSIR of India are acknowledged for fellowship.

Supporting information for this article is available on the WWW under http://dx.doi.org/10.1002/anie.201210277.

are observed lying vertically, the height of these platelets is calculated to be ca. 6–7 nm (Figure S2).

For the characterization of these nanoplatelets, we have carried out elemental analysis and analyzed the HRTEM and XRD images of the samples. From energy-dispersive X-ray spectroscopy (EDAX), we have observed that these platelets contain Cu and P elements and their ratio is approximately 3:1. Figure 2a shows the HRTEM of a single platelet of ca. 200 nm width. The calculated d spacing of 0.203 nm supports the planes of trigonal Cu_3P. The fast Fourier transform (FFT; Figure 2b) suggests that the planes are {030} group of planes and the platelet is viewed along the Z or [001] direction. The atomic pattern of the platelet viewed along the Z direction is shown in Figure 2c. The XRD pattern shown in Figure 2d

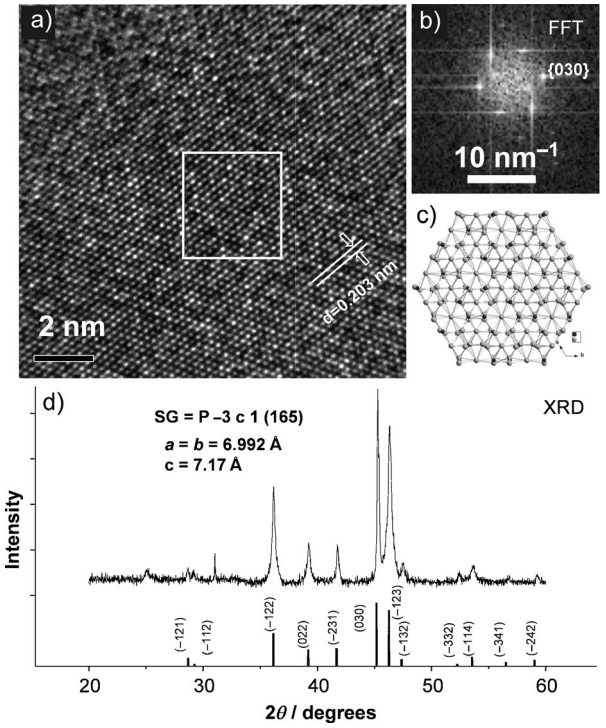

Figure 2. a) HRTEM image of a Cu_3P platelet. b) The FFT of the white-marked square area. For additional HRTEM images and for the platelet from which the HRTEM image was obtained, see Figure S3. c) Atomic model representation of the HRTEM viewed along the [001] direction. The model is based on data collected from ICSD no. 26775. d) XRD image of Cu_3P platelets (width ca. 200 nm).

also shows the peak positions overlapping with the trigonal crystal phase of bulk Cu_3P. So, the hexagonal platelets synthesized can be confirmed to be Cu_3P with a trigonal phase.

Analysis of the reaction parameters presented in Table S1 suggests that the platelets obtained after the same time (10 min) from different reactions and showing different sizes only vary in trioctylphosphine (TOP) concentration. Both alkylamine and trioctylphosphine oxide (TOPO) act as the solvent only. Importantly, it has been observed that even samples collected after two minutes show platelets of similar size in each case (Figure S4). Hence, the 2D growth is observed to be much faster here. However, in TEM grids obtained by placing almost equal sample amounts following similar dilution of the total samples collected from two different reactions, and having platelets with ca. 200 nm and ca. 900 nm width, it has been observed that only a few platelets are found in later case (Figure S5). This suggests that the number of nucleations in the case of the wider platelets is limited relative to the smaller platelets. This has been further verified from the OD difference of the equal amount of samples collected from different reaction systems (Figure S6). The back calculation of the unreacted Cu amount also suggests that the number of nucleations varies with variation of the TOP amount (see the Supporting Information for details).

Furthermore, as TOP was found to be the only variable parameter for obtaining different platelet sizes, we can assume that a higher amount of TOP decreases the number of nucleations. However, unlike in an earlier report,[32] TOP here does not act as the phosphide source; without TOP, platelets are also obtained, although with wider size distribution (Figure S7). Also, reaction only with TOP (without phosphine gas) does not form the platelets under these reaction conditions. TOP, being a soft base, can form a complex with Cu, which is a soft acid,[33–35] and thus reduces the activity of the Cu precursor, which in turn limits the number of nucleations. But, as crystal growth requires lower energy than the formation of nucleations, the presence of TOP does not affect this growth process. Moreover, 2D growth along the X and Y directions of the platelets is observed to be so much faster that TOP may not be able to control the same. To further confirm this, the nucleation temperature of the reaction was increased to 280 °C instead of 230 °C. Surprisingly, the width of the platelets is limited to 200–300 nm instead of ca. 900–1000 nm. This suggests that higher reaction temperature takes over control of nucleation, which is then no longer affected by TOP. Hence, in our optimized reaction temperature, TOP controls the reactivity of Cu ions and reduces the number of nucleations, which helps in obtaining the wide tunable size range of platelets. As the 2D growth is much faster, it could not be decoupled from the nucleation, as in the conventional colloidal synthesis of nanocrystals, and hence nanoplatelets collected at consecutive time intervals did not show any difference in their dimensions. On the contrary, to obtain different sizes, different reactions were performed, in which the number of nucleations of the platelets were varied to obtain the wide tunability.

One of the important observations here is the crystallinity of the platelets, although the reactions are carried out at relatively moderate temperatures. Both HRTEM and XRD indicate single-crystallinity of the platelets. This has been further supported by several intriguing patterns of the Moiré fringes obtained at the overlapping regions of multiple platelets. Figure 3a presents both isolated and overlapping platelets, and the patterns are observed in the latter case. HRTEM of one of the overlapped platelets showing both the single platelet and the overlapped area is shown in Figure 3b. The FFT of the single platelet region shows a d spacing of 0.203 nm, which corresponds to planes of Cu_3P. On the other

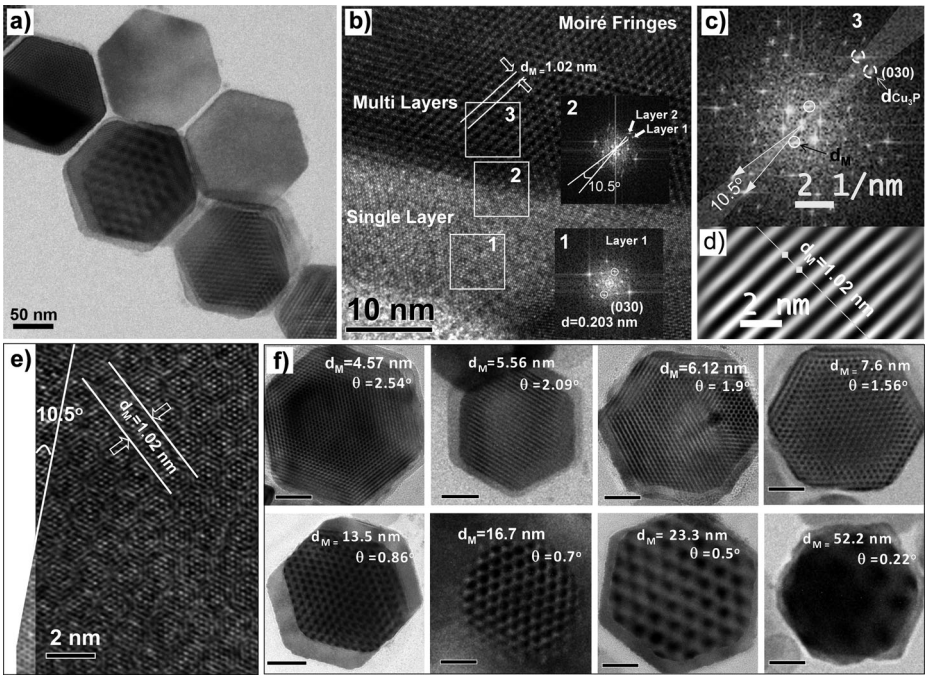

Figure 3. a) TEM image of the Cu_3P platelets showing Moiré patterns. b) HRTEM image of single and overlapped platelets. Insets show the selected area FFT pattern of the area marked by white squares 1 and 2. c) FFT of the area marked by white square 3 in panel (b). d) Simulated Moiré planes. e) Overlapped model of the HRTEM of two platelets at an angle of 10.5 degrees. f) TEM images of different overlapped platelets showing Moiré patterns with varying Moiré d-spacing (inserts). The angle in each case has been calculated following the equation $d_M = d/(2\sin\theta/2)$; where d_M is the Moiré d-spacing and d = Cu_3P d-spacing (0.203 nm). Scale bars are 50 nm. HRTEM images of more overlapping platelets are given in Figure S8.

hand, the FFT from the border and the overlapped region clearly suggests that the two platelets are overlapped at an angle of 10.5 degrees (Figure 3c). To confirm this, we have simulated the FFT pattern considering the two neighboring bright spots, as marked in Figure S9. The simulated Moiré pattern from the FFT is also been shown in Figure 3d. Moreover, we rotated two HRTEM images of the platelets at 10.5 degrees (Figure 3e) and back calculated the Moiré d spacing; the spacing ($d_M = 1.02$ nm) remains the same as that measured in Figure 3b.

Although Moiré fringes are very common and are supposed to be obtained at the overlapping regions of two sheets or platelets, we observed here practically the same with several interesting patterns. To our knowledge, the case here is unique among previous reports on Moiré fringes[28,36–38] and we assume this to be because of the highly crystalline nature of the platelets. Figure 3f presents several Moiré patterns with d spacing (d_M) in the range of ca. 4.57–52.2 nm. The rotation angles (θ) between two platelets are also shown in each panel of the figure, along with the respective d_M spacing.

It has been observed that these platelets are associated with several important and useful materials properties. Figure 4a shows the optical absorption spectra, which indicates that these platelets absorb in the NIR region; this makes them a possible candidate for photovoltaics that absorb solar light. No sharp absorption peaks are obtained, possibly owing to the indirect bandgap of the materials. The calculated extinction coefficient[39] (calculated at 610 nm) remains $4\times10^6\,cm^{-1}M^{-1}$ for ca. 100 nm size platelets. As the platelets have much larger width, quantum confinement effects are not observed. The approximate calculation from the band edge suggests that the bandgap remains ca. 1.3 eV and this has further been confirmed by scanning tunneling spectroscopy (STS). However, what is most important is the additional tunable absorption in the mid-IR region (shown in Figure 4b). This absorption has been observed to be tunable, and to vary in intensity when trailed to lower energy. Similar absorption in this region has previously been reported for Cu_2S and Cu_2Se, and is mostly due to localized surface plasmon resonance (LSPR).[5–8,18] However, this has been observed for the first time in Cu_3P. This plasmonic absorbance is further supported by the tuning of the absorption energy with variation of the dispersion mediums of different refractive index. A typical example of solutions in CCl_4, CS_2, and C_2Cl_4 suggests that the absorption

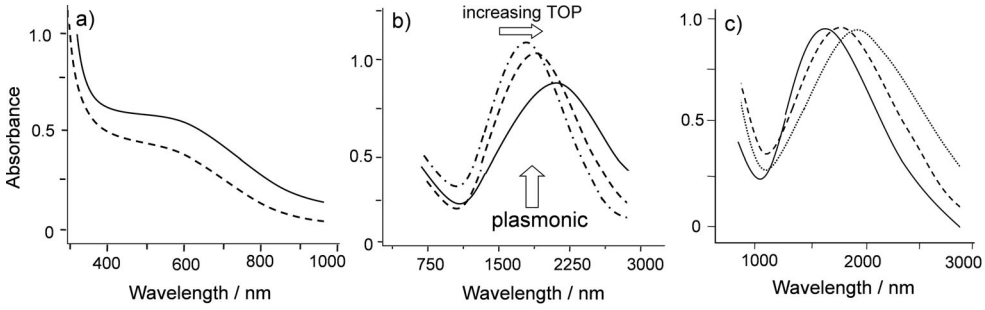

Figure 4. a) Absorption spectra of Cu_3P nanoplatelets with ca. 100 (-----) and ca. 500 nm (——) average widths. b) Absorption spectra in C_2Cl_4 with extended scale, showing the plasmonic absorption for platelets of 10–50 nm (–•–•), 200–250 nm (-----), and 400–500 nm (——). The spectra shown include variation of TOP, as well as size. c) Tunability of the plasmonic absorption through variation of the refractive index (RI) of the solvent. RI for CCl_4 (——), C_2Cl_4 (-----), and CS_2 (••••) are 1.46, 1.51, and 1.62, respectively. The platelet sizes remain ca. 50–100 nm.

position varies from one to the other (Figure 4c). This effect has earlier been shown for copper sulfide nanocrystals.[5]

The plasmonic absorption arises because of the presence of free charge carriers (holes) in the nanocrystals.[5,6] The probable reason for tuning of LSPR is the Moss–Burstein effect,[40,41] which states that the increase in the number of charge carriers effectively lowers the energy of the valence band and increases the optical bandgap. These charge carriers are generated from copper vacancies, which arise from the nonstoichiometric composition of the nanomaterial.[5–7,19] The use of strong surface binding ligands such as TOP and TOPO has been reported to produce a stoichiometric compound with fewer copper vacancies,[8,42] which results in a red-shifted LSPR without changing the size of the nanocrystal. In our case, we also observed that increasing TOP causes a red shift in the plasmonic absorbance, indicating that an increase in TOP leads to the formation of stoichiometric Cu_3P platelets. Again, the intensity of the plasmonic peak is also proportional to the charge carrier concentration,[6] and hence to copper vacancies. So a decrease in TOP leads to an increase in plasmonic intensity along with a blue shift of the peak. Fortunately, we also observed that the size of the platelets also increases as TOP concentration increases. To distinguish the size and TOP concentration effects on the plasmonic shift, we carried out a control reaction for the ca. 400–500 nm platelets at 260 °C instead of 230 °C, keeping all other conditions same. We obtained ca. 200–300 nm platelets whose plasmonic absorption was observed to be broad and overlapped with the larger (ca. 400–500 nm) platelets. This suggests that the plasmonic peak position is more affected by the concentration of TOP than by the size. However, as the plasmonic absorption in these semiconductors is a new observation, the determination of its origin requires further investigation and supporting data.

These materials are explored to study their photocurrent, photoresponse, and photovoltaic properties. Figure 5a shows the *I–V* characteristics of a thin film of Cu_3P nanocrystals both in the dark and in the presence of light. These devices were fabricated with a layered structure composed of ITO/PEDOT:PSS/Cu_3P/Al (ITO = indium tin oxide, PEDOT:PSS = poly(3,4 ethylenedioxythiophene)poly(styrenesulfonate)). The observed plots in dark and light suggest that, in presence of white light, the flow of current increases. Similarly, the photoresponse of this film was measured by periodically turning the light on and off, and the plot is shown in Figure 5b. This device was fabricated after ligand exchange of the platelets with shorter amines.[4] It shows that the dark current (3×10^{-6} A) increases sharply to 2.4×10^{-5} A when the light source is turned on, which suggests fast photodetection by Cu_3P. Furthermore, a device with a p–n junction has been explored to study the rectification behavior of the platelets. From STS, the bandgap and band positions in vacuum were calculated (Figure S10), and it was observed that the bandgap of these materials remains within 1.3–1.4 eV. Considering their band positions, a device was fabricated from these p-type materials with CdS as the n-type material (ITO/PEDOT:PSS/Cu_3P:CdS/Al). The relative band position of Cu_3P and CdS is given in Figure 5c. The measured *I–V* in Figure 5d shows the rectification behavior (efficiency = 0.49 %) and this suggests that this material can also be used for photovoltaic applications. Details of the fabrication of the device are shown in the supporting information.

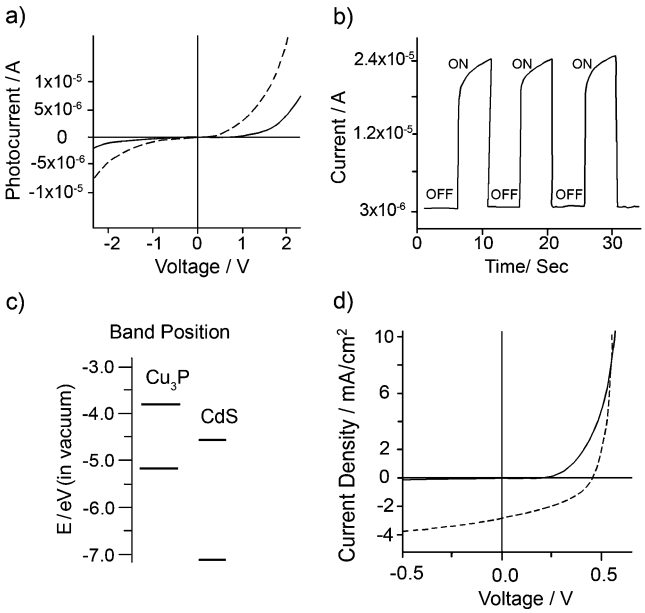

Figure 5. a) *I–V* characteristics of the photodetector ITO/PEDOT:PSS/Cu_3P/Al in the dark (——) and under illumination (-----; Xe lamp) using a 2 V bias and 100 mW cm^{-2} white-light intensity. b) Photocurrent response of the photodetector using the white-light source. This has been performed up to three cycles and for all cycles it behaves the same. c) Band positions of Cu_3P and CdS. d) *I–V* characteristics of a photovoltaic device with a Cu_3P–CdS p–n junction based on Cu_3P nanoplatelets with a layered structure of ITO/PEDOT:PSS/Cu_3P:CdS/Al, in the dark (——) and under white-light illumination conditions (-----). Open circuit voltage (V_{OC}) = 0.46, short circuit current density (I_{SC}) = 2.7, fill factor (FF) = 0.39, efficiency = 0.49 %.

In summary, we report a moderate and relatively low temperature synthetic method for obtaining 2D platelet-shaped Cu^I phosphide semiconducting and plasmonic materials. This synthetic method allows for wide tunable control of platelet size from nanometer (ca. 10 nm) to micrometer (ca. 1000 nm) scale. These platelets are single crystalline and show Moiré patterns upon overlapping. Moreover, these platelets possess the semiconducting, plasmonic, and rectification properties that are the properties required for developing technologies. Preliminary results of the photocurrent, photoresponse, and photovoltaic activity also demonstrate the widespread potential applications of the material.

Received: December 25, 2012
Revised: March 7, 2013

Keywords: Copper · Moiré fringes · nanostructures · photovoltaic · plasmonic

[1] I. Robel, V. Subramanian, M. Kuno, P. V. Kamat, *J. Am. Chem. Soc.* **2006**, *128*, 2385.

[2] Y. Wu, C. Wadia, W. Ma, B. Sadtler, A. P. Alivisatos, *Nano Lett.* **2008**, *8*, 2551.
[3] S. A. McDonald, G. Konstantatos, S. Zhang, P. W. Cyr, E. J. D. Klem, L. Levina, E. H. Sargent, *Nat. Mater.* **2005**, *4*, 138.
[4] J. Tang, G. Konstantatos, S. Hinds, S. Myrskog, A. G. Pattantyus-Abraham, J. Clifford, E. H. Sargent, *ACS Nano* **2009**, *3*, 331.
[5] J. M. Luther, P. K. Jain, T. Ewers, A. P. Alivisatos, *Nat. Mater.* **2011**, *10*, 361.
[6] Y. Zhao, H. Pan, Y. Lou, X. Qiu, J. Zhu, C. Burda, *J. Am. Chem. Soc.* **2009**, *131*, 4253.
[7] D. Dorfs, T. Hartling, K. Miszta, N. C. Bigall, M. R. Kim, A. Genovese, A. Falqui, M. Povia, L. Manna, *J. Am. Chem. Soc.* **2011**, *133*, 11175.
[8] X. Liu, X. Wang, B. Zhou, W.-C. Law, A. N. Cartwright, M. T. Swihart, *Adv. Funct. Mater.* **2013**, *23*, 1256.
[9] Q. Sun, Y. A. Wang, L. S. Li, D. Wang, T. Zhu, J. Xu, C. Yang, Y. Li, *Nat. Photonics* **2007**, *1*, 717.
[10] V. Wood, M. J. Panzer, J.-M. Caruge, J. E. Halpert, M. G. Bawendi, V. Bulovic, *Nano Lett.* **2010**, *10*, 24.
[11] R. Beaulac, L. Schneider, P. I. Archer, G. Bacher, D. R. Gamelin, *Science* **2009**, *325*, 973.
[12] U. I. Tromsdorf, N. C. Bigall, M. G. Kaul, O. T. Bruns, M. S. Nikolic, B. Mollwitz, R. A. Sperling, R. Reimer, H. Hohenberg, W. J. Parak, S. Foerster, U. Beisiegel, G. Adam, H. Weller, *Nano Lett.* **2007**, *7*, 2422.
[13] H. B. Na, J. H. Lee, K. An, Y. I. Park, M. Park, I. S. Lee, D.-H. Nam, S. T. Kim, S.-H. Kim, S.-W. Kim, K.-H. Lim, K.-S. Kim, S.-O. Kim, T. Hyeon, *Angew. Chem.* **2007**, *119*, 5493; *Angew. Chem. Int. Ed.* **2007**, *46*, 5397.
[14] A. Kongkanand, K. Tvrdy, K. Takechi, M. Kuno, P. V. Kamat, *J. Am. Chem. Soc.* **2008**, *130*, 4007.
[15] E. J. D. Klem, D. D. MacNeil, L. Levina, E. H. Sargent, *Adv. Mater.* **2008**, *20*, 3433.
[16] E. H. Sargent, *Adv. Mater.* **2008**, *20*, 3958.
[17] A. J. Nozik, J. Miller, *Chem. Rev.* **2010**, *110*, 6443.
[18] S.-W. Hsu, K. On, A. R. Tao, *J. Am. Chem. Soc.* **2011**, *133*, 19072.
[19] S.-W. Hsu, W. Bryks, A. R. Tao, *Chem. Mater.* **2012**, *24*, 3765.
[20] M. Kruszynska, H. Borchert, A. Bachmatiuk, M. H. Ruemmeli, B. Buechner, J. Parisi, J. Kolny-Olesiak, *ACS Nano* **2012**, *6*, 5889.
[21] G. Garcia, R. Buonsanti, E. L. Runnerstrom, R. J. Mendelsberg, A. Llordes, A. Anders, T. J. Richardson, D. J. Milliron, *Nano Lett.* **2011**, *11*, 4415.
[22] J. S. Niezgoda, M. A. Harrison, J. R. McBride, S. J. Rosenthal, *Chem. Mater.* **2012**, *24*, 3294.
[23] C. Schliehe, B. H. Juarez, M. Pelletier, S. Jander, D. Greshnykh, M. Nagel, A. Meyer, S. Foerster, A. Kornowski, C. Klinke, H. Weller, *Science* **2010**, *329*, 550.
[24] N. Pradhan, S. Efrima, *J. Phys. Chem. B* **2004**, *108*, 11964.
[25] A. P. Alivisatos, *Science* **1996**, *271*, 933.
[26] Z. A. Peng, X. Peng, *J. Am. Chem. Soc.* **2002**, *124*, 3343.
[27] Z. A. Peng, X. Peng, *J. Am. Chem. Soc.* **2001**, *123*, 1389.
[28] D. D. Vaughn, S.-I. In, R. E. Schaak, *ACS Nano* **2011**, *5*, 8852.
[29] H. Park Kang, K. Jang, U. Son Seung, *Angew. Chem.* **2006**, *118*, 4724; *Angew. Chem. Int. Ed.* **2006**, *45*, 4608.
[30] M. B. Sigman, Jr., A. Ghezelbash, T. Hanrath, A. E. Saunders, F. Lee, B. A. Korgel, *J. Am. Chem. Soc.* **2003**, *125*, 16050.
[31] L. Li, M. Protiere, P. Reiss, *Chem. Mater.* **2008**, *20*, 2621.
[32] L. De Trizio, A. Figuerola, L. Manna, A. Genovese, C. George, R. Brescia, Z. Saghi, R. Simonutti, M. Van Huis, A. Falqui, *ACS Nano* **2012**, *6*, 32.
[33] J. M. Luther, H. Zheng, B. Sadtler, A. P. Alivisatos, *J. Am. Chem. Soc.* **2009**, *131*, 16851.
[34] K. Miszta, D. Dorfs, A. Genovese, M. R. Kim, L. Manna, *ACS Nano* **2011**, *5*, 7176.
[35] B. Sadtler, D. O. Demchenko, H. Zheng, S. M. Hughes, M. G. Merkle, U. Dahmen, L.-W. Wang, A. P. Alivisatos, *J. Am. Chem. Soc.* **2009**, *131*, 5285.
[36] V. Luchnikov, A. Kondyurin, P. Formanek, H. Lichte, M. Stamm, *Nano lett.* **2007**, *7*, 3628.
[37] S. Acharya, M. Dutta, S. Sarkar, D. Basak, S. Chakraborty, N. Pradhan, *Chem. Mater.* **2012**, *24*, 1779.
[38] G. Trambly de Laissardière, D. Mayou, L. Magaud, *Nano Lett.* **2010**, *10*, 804.
[39] W. W. Yu, L. Qu, W. Guo, X. Peng, *Chem. Mater.* **2003**, *15*, 2854.
[40] T. S. Moss, *Proc. Phys. Soc. B* **1954**, *67B*, 775.
[41] E. Burstein, *Phys. Rev.* **1954**, *93*, 632.
[42] S. C. Riha, D. C. Johnson, A. L. Prieto, *J. Am. Chem. Soc.* **2011**, *133*, 1383.